Dynamic neutron radiography studies of drying of kaolin clay cylinders*

Izabela Fijał-Kirejczyk,
Jacek J. Milczarek,
Jacek Banaszak,
Andrzej Trzciński,
Joanna Żołądek

Abstract. The results of neutron radiography studies on convective drying of kaolin cylinders are presented. The sample shrinkage and loss of water during drying was easily observed on registered neutron radiograms. The saturation of the sample with water was estimated in terms of the neutron effective macroscopic cross-section. The results are comparable to those of gravimetric measurements and are discussed within the framework of simple theories of drying. The effect of the scattered neutrons is discussed in terms of the results of the MC simulations.

Key words: drying • kaolin • neutron radiography

I. Fijał-Kirejczyk✉, J. J. Milczarek, J. Żołądek
Institute of Atomic Energy,
05-400 Otwock/Świerk, Poland,
Tel.: +48 22 7180060, Fax: +48 22 8105960,
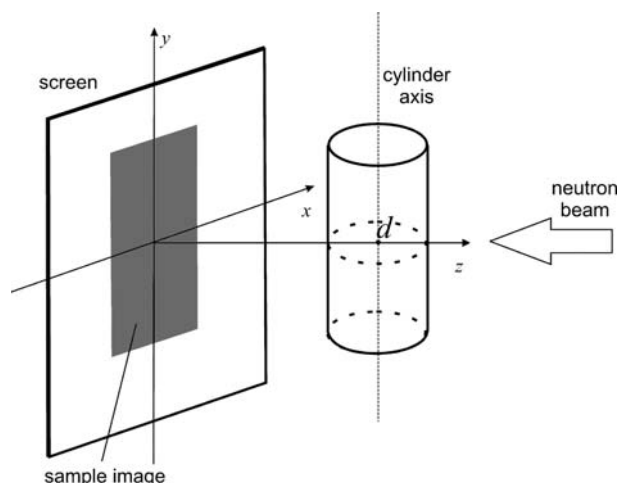E-mail: i.fijal@cyf.gov.pl

J. Banaszak
Institute of Technology and Chemical Engineering,
Poznań University of Technology,
2 M. Skłodowskiej-Curie Sq., 60-965 Poznań, Poland

A. Trzciński
The Andrzej Sołtan Institute for Nuclear Studies,
05-400 Otwock/Świerk, Poland

Introduction

Drying of items formed into desired shapes is one of the important processes used in many industries [1, 15, 16, 21]. The process usually consists in removing of water from the body by evaporation from its surface. The loss of water leads to shrinking, which changes product size and shape. The rate of loss of water during drying is one of the most important factors describing various stages of the process [1, 2, 15, 16, 21, 22, 24].

The aim of the present work was to obtain experimental data on the drying of simple cylindrical samples of kaolin clay with dynamic neutron radiography (DNR). This non-destructive technique has been proved to be perfect for studies of invasion of water into media of different kinds. In particular, DNR is invaluable in determination of the wetting front motion and water distribution inside the rigid and granular porous media [3, 5, 7, 8, 11, 17–19]. We hope that the results of our experiments on drying will provide useful data for quantitative considerations of the drying process.

It is well known that the drying consists of evaporation at the surface which entails the transport of the water from the inner regions of the specimen to its surface [1, 2, 15, 16, 21, 22, 24]. The transport is driven by capillary forces and diffusion induced by the gradient of the water content increasing toward the surface. Most of the theoretical treatments of the subject are based on continuum mechanics of viscoelastic materials [16, 21]. The simplest mathematically tractable case is

Fig. 1. Sketch of the sample arrangement with respect to the converter screen in the neutron radiography station.

the spherical sample dried in isotropic conditions [16]. However, due to difficulties in producing and supporting such samples, most experiments are performed on cylinders dried by air convection at ambient temperature. In our experiments on the cylindrical samples the change in water content and in sample sizes were determined from the neutron radiograms recorded on line during drying.

Experiments and data analysis

The experiments were performed on cylindrical samples prepared from wet kaolin clay. The appropriate amounts of clay and tap water were mixed together in order to obtain material with ~ 30% mass content of water. The corresponding volumetric water content in the sample reached ~ 50% i.e. the full saturation of the porous medium. The clay mold was kept in an impermeable vessel for 24–72 h and then stirred for a short time just before preparation of samples. The cylindrical samples of 12–35 mm in diameter and 25–35 mm in height were manufactured by extrusion and immediately placed at neutron radiography sample table with its axis at a distance d of ~ 35 mm from the converter screen (Fig. 1). Due to high moisture content some buckling of the samples at the bottom was observed. Here, we report the results of two experiments with two different sample sizes and methods of drying employed. In the first one the sample was dried at the sample table of

NR station at ambient temperature of 22°C. The second experiment consisted of repeated cycles of drying and observations. The sample was dried for some time in a furnace at 95°C, then moved from the furnace, weighed and observed for an 8 min period at the station and then placed again in the furnace.

Experiments were performed with the previously described standard DNR station located at the nuclear research reactor MARIA of IAE [3, 4, 7, 8, 18]. The system comprises neutron beam collimators, fluorescent screen (250 × 250 mm), mirror, optical zoom lenses and high sensitive CCD camera. The main components of the system are: an AST NDg ^{6}Li:ZnS:Cu,Al,Au screen and a Hammamatsu ORCA-ER high-sensitivity camera (1280 × 1024 pixels, 12 bits). The collimating L/D ratio during reported experiments was ~ 165. The exposure time of 1.6 s was applied and the radiograms were acquired periodically during the observed processes. The projection ratio provided by the optical system was 154 μm/pixel determined with the application of a Cd 80 mm long standard plate. For image analysis, the LUCIA™ 4.60 software was used. The preprocessing of the analyzed images consisted in the correction of brightness for the black current and the median filter correction in order to eliminate white spots. The values of brightness B discussed further on in this work are the corrected values.

The on-line registered neutron radiograms reveal shrinking of the sample and an increase of brightness within the sample image (Fig. 2) during drying. The size of the sample was determined from the analysis of the distribution of brightness over the collected frames. To analyze the changes of the brightness B_{exp} over the image we took into account the distribution of brightness B_0 recorded with no sample on the table. The plot of the ratio $b = B_{exp}/B_0$ of these two variables along the line perpendicular to the sample axis has the shape of the well with walls corresponding to the sample edges (Fig. 3). At the beginning of the drying, the well has almost rectangular shape but it gets shallow and more rounded with increasing drying time.

The radius R of the sample decreases initially at an almost constant rate and does not change in the further stage (Fig. 4). This observation corresponds to the well known feature [1, 2, 16, 21, 22, 24] of drying that in the initial period the rate of water loss is independent of time. Our results indicate that the duration of the constant rate period (CRP) decreases with increasing temperature.

In order to get information on the water content distribution over the sample the distribution of bright-
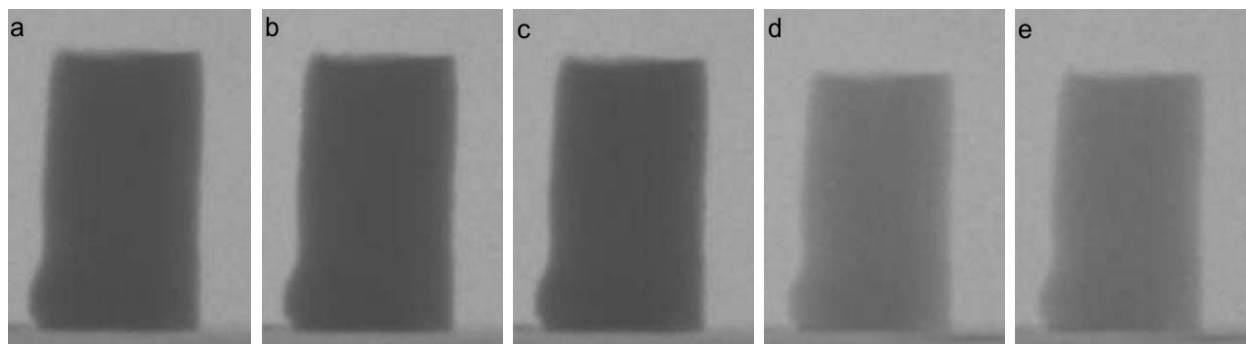
Fig. 2. Examples of neutron radiograms of drying kaolin cylinder for different time of the process. The pictures a, b, c, d, e correspond to 0.5, 3, 7, 20, 25 h after beginning of drying, respectively.
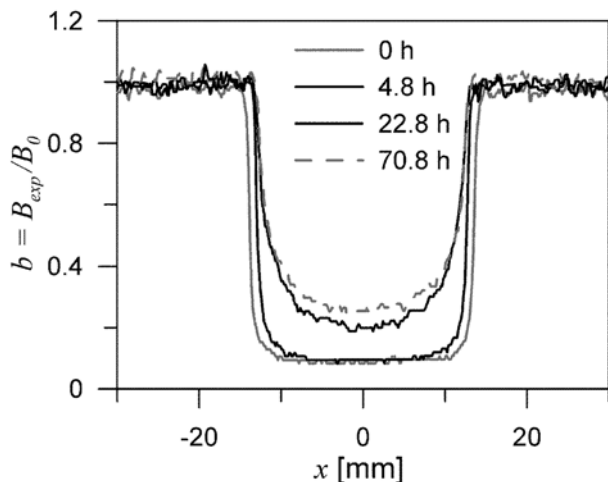
Fig. 3. Example of the evolution of spatial distribution of relative brightness $b = B_{exp}/B_0$ determined along the line perpendicular to the sample axis at the half of its height.

ness over the specimen was analyzed. We found that the presence of water reduces the brightness in the central region of the sample image by a factor of ~ 3 in comparison to the image of the dry sample (Fig. 3). One should bear in mind that for precise analysis the neutron attenuation produced by water is due predominantly to strong incoherent scattering of neutrons, the effect that also increases brightness in the central part of the samples' image [5, 9–12, 14, 17, 23]. The first step in our analysis consists in the consideration of the neutron absorption described by the macroscopic neutron cross-section related to the optical density which is simply $\ln(B_0/B_{exp})$ [5–8, 11–13, 17, 23]. Assuming perfect collimation of the incident neutron beam, the effective macroscopic neutron cross-section Σ_{eff} within the sample was calculated as the ratio of optical density and the sample width at the position x

(1) $$\Sigma_{eff} = \frac{\ln(B_0/B_{exp})}{d_{12}} = \frac{\ln(B_0/B_{exp})}{\sqrt{R^2 - x^2}}$$

where x is the position in the image on the line perpendicular to the sample axis and parallel to the screen
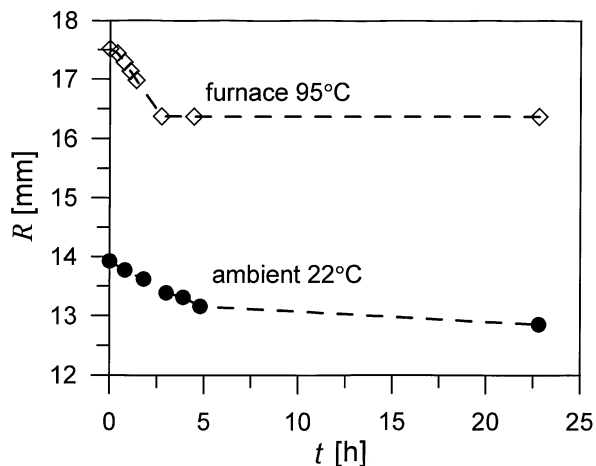
Fig. 4. Time dependence of the sample radius for drying at 22°C in ambient air and at 95°C in a furnace.
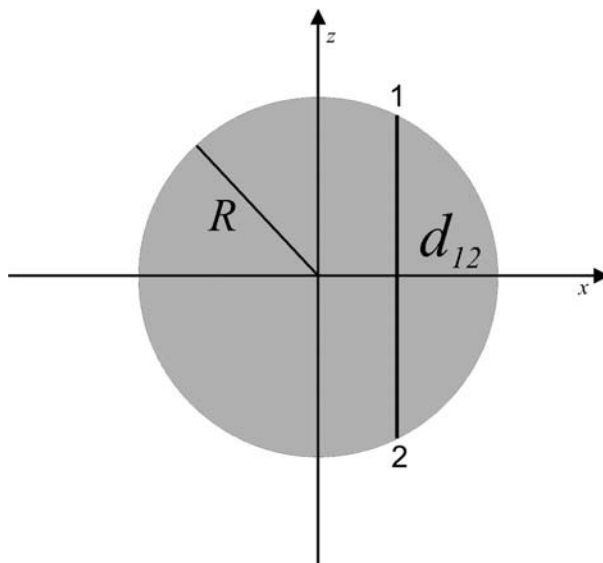

Fig. 5. Sketch of the cross-section of the sample with the plane perpendicular to the converter screen plane.

plane, and $|x| < R$ (Fig. 5). We assume here and further on that the position of the cylinder axis coincides with $x = 0$. The shape of the plots of the effective cross-section vs. position depends on the time of drying. During the CRP, the two maxima ("horns") at sample edges are observed, whereas for further stages the plot is of almost rectangular shape with flat top (Fig. 6).

Since the effect of the side maxima in $\Sigma_{eff}(x)$ plots persists for several hours during drying and the migration of water in clay samples of ~ 100 mm height does not depend on the gravity [19], the gravity-induced leakage of the water through the side surface of the sample should be totally excluded as the source of the maxima.

Model calculations and discussion

The minimum observed in the macroscopic cross-section distribution across sample is due to neutron scattering that produces the "build-up effect" observed and discussed thoroughly for parallelepiped layers of water [5, 9–11, 14, 17, 20, 23]. The analysis of this effect should be based on some model calculations of the imaging process [9, 10, 14, 23].
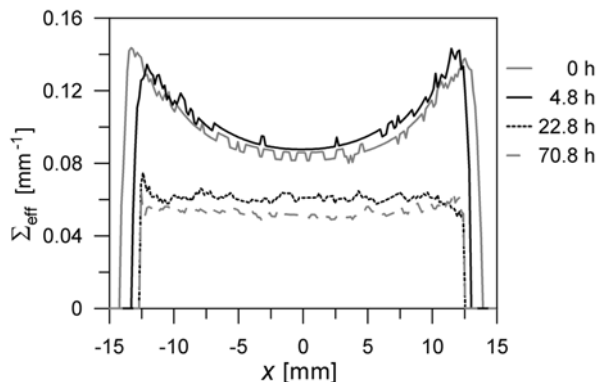
Fig. 6. Evolution of the spatial distribution of the effective macroscopic neutron cross-section determined along the line perpendicular to the sample axis.
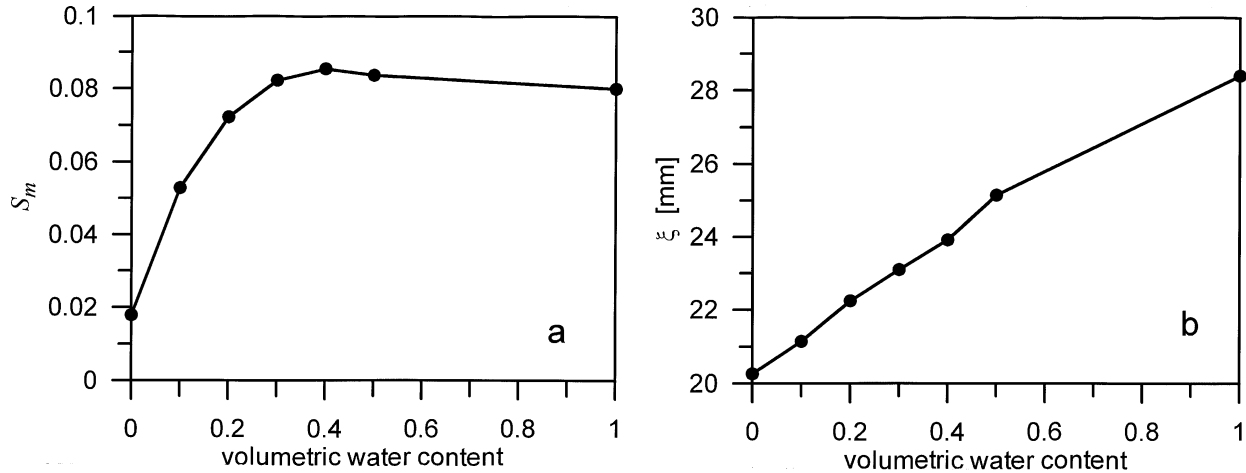
Fig. 7. The dependence of the amplitude of the scattered neutron component (a) and its half-width (b) on the volumetric water content calculated in MC simulations for a porous Al_2O_3 cylinder.

It can be proved that the neutron absorption does not produce such effect for any axially symmetric distribution of water inside the sample volume consistent with the condition of its decreasing with distance r from the cylinder axis. To this end, we start from the definition of the effective macroscopic cross-section at point x for a cylinder of radius R and the long axis parallel to the screen plane (Figs. 1 and 5):

$$(2) \qquad \Sigma_{eff} = \frac{1}{d_{12}} \int_1^2 \Sigma(r) dz$$

where d_{12} is the length of a line segment projecting the cylinder along the line perpendicular to the screen at point x from the cylinder's axis (Fig. 5). The neutron attenuation is proportional to the water content, which decreases towards sample boundary during drying. For simplicity, we assume that the macroscopic cross-section decreases as square in r:

$$(3) \qquad \Sigma(r) = \Sigma_0 - sr^2$$

In effect, we get that the observed macroscopic cross-section $\Sigma_{eff}(x)$ also decreases with distance x from the cylinder axis

$$(4) \qquad \Sigma_{eff}(x) = \left(\Sigma_0 - \frac{s}{3}R^2 \right) - \frac{2}{3}sx^2$$

The analysis of the scattered neutron components for cylinders is more intricate and needs some more elaborate calculations. In order to discuss the contribution of the scattered neutrons to the brightness we performed the Monte Carlo (MC) simulations of the image formation using the MSX code [20] for the arrangement specified in Fig. 1. The neutron beam consisting of parallel neutrons running in the direction normal to the screen plane was illuminating the cylinder. The calculations were carried out for the cylinder of diameter 25 mm and 30 mm height with its axis 30 mm apart from the screen. The cylinder contained a ternary mixture of Al_2O_3, water and air. The corundum content was fixed at 50% volume, and the water saturation was varied from 10 to 50% of volume with its rest filled with air. The results of the MC simulations revealed that

the scattered neutrons distribution along the Ox axis (perpendicular to the cylinder axis at its half height) can be described by the Lorentzian with amplitude S_m and half-width ξ:

$$(5) \qquad S(x) = \frac{S_m}{1 + (x/\xi)^2}$$

The amplitude S_m was found to increase initially with increasing water content and to level off at a volumetric water content higher than 25% of volume (Fig. 7a) with a slight decrease in the value of cylinder filled totally with water. The half-width ξ is proportional to the water content (Fig. 7b).

Assuming that the relative brightness $b(x) = B(x)/B_0(x)$ at the point x is proportional to the sum of the number of neutrons impinging the screen without leaving their rectilinear trajectories and the scattered neutrons

$$(6) \qquad b(x) = \exp(-2\Sigma\sqrt{R^2 - x^2}) + S(x)$$

the parameters Σ, S_m and ξ were estimated from the fits to the experimental B/B_0 profiles (Fig. 3). We found the results of fits consistent with the MC calculations (Fig. 8).
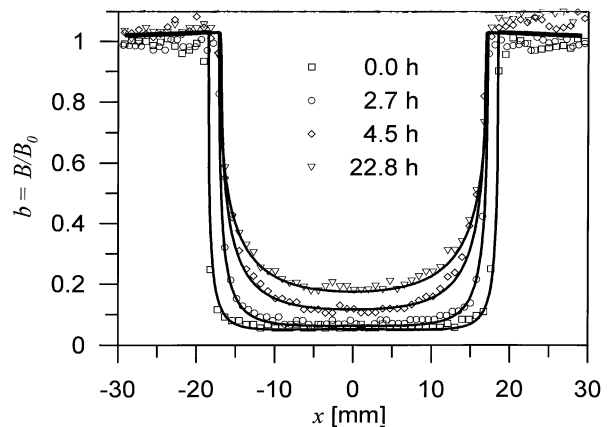
Fig. 8. Examples of the fits (solid lines) of the formula (6) to the experimental profiles (symbols) of the relative brightness for the sample dried at a furnace at 95°C.
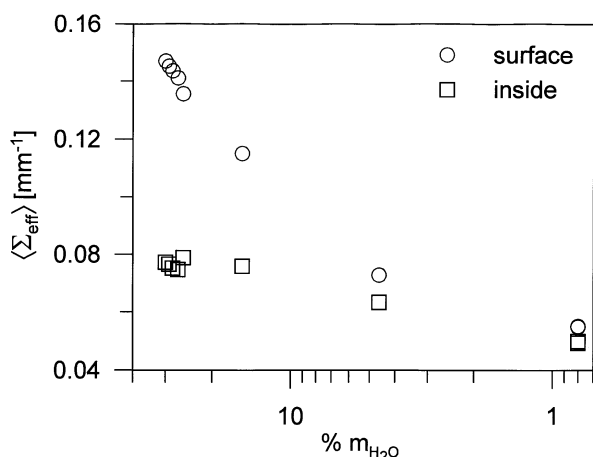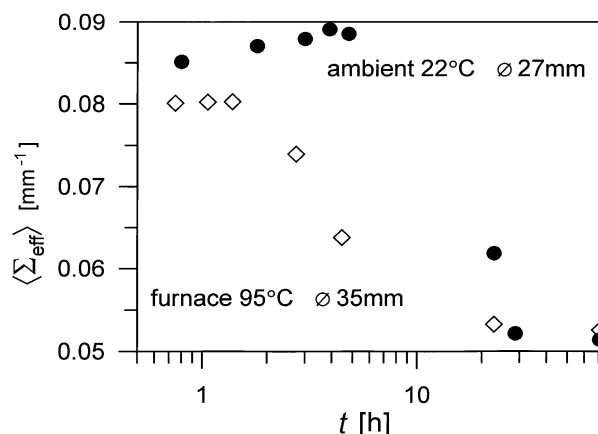
Fig. 9. The dependence of the average macroscopic neutron cross-section in the middle and at the boundary of the sample on the mass content of the water for forced drying procedure at 95°C. Note the inverted scale of the horizontal axis.

Fig. 10. Time dependence of the effective macroscopic neutron cross-section determined for the central region of the sample.

Some of the quantitative results on the rate of the drying process can be attained without the analysis of the contribution of the neutron scattering. We estimated the evolution of the water saturation in the central part of the sample by averaging Σ_{eff} over the central region of 3 mm × 3 mm size. The evolution of the water content near the sample boundary surface was estimated by averaging Σ_{eff} in the thin boundary region of 3 mm × 0.5 mm in the half-height of the sample. The obtained time dependence of the average $\langle\Sigma_{eff}\rangle$ reveals two stages of the drying process. The $\langle\Sigma_{eff}\rangle$ is constant or slightly increases in the first stage and decreases significantly during the second stage (Fig. 9). This effect is consistent with common description and model calculations of the kinetics of drying of cylinders [16, 21]. The water content of the cylinder innermost region does not change in the CRP of drying. The central parts of the sample loose water in the phase called falling rate period (FRP) since the rate of drying is suppressed during that stage.

We should note that the same value of $\Sigma_{eff} \approx 0.052$ mm^{-1} was determined for dry kaolin clay cylinders independently of the cylinder size and the drying procedure (Fig. 10).

The slight increase in the $\langle\Sigma_{eff}\rangle$ revealed for low temperature drying (Fig. 10) can be attributed to two effects due to fast drying and shrinkage of the sample outer layer. The first reason is that the average macroscopic cross--section calculated according to Eq. (1) for the central region of the sample image increases since the amount of moisture in the inner region of the sample does not change during CRP, but the radius is rapidly decreasing. The second explanation is based on the decreasing contribution of neutron scattering due to loss of water in the outer skin of the sample. This effect yields suppression of brightness in the central part. However, the quantitative evaluation of both effects should be performed on the basis of the model calculations.

For the sample dried in the furnace at 95°C, we can check the correlation between the sample mass and $\langle\Sigma_{eff}\rangle$ (Fig. 9). The presence of the CRP is discernible since the $\langle\Sigma_{eff}\rangle$ does not change with mass of the sample for this period. Let us note that the decrease in the mass of water

contained in the sample is accompanied by the decrease of the average macroscopic cross-section in the FRP.

Summary

We have demonstrated the applicability of neutron radiography for studies of the drying process of kaolin clay items. The main aim of obtaining data on the kinetics of the process was achieved. The two commonly recognized stages of the drying process, namely the constant (drying) rate period and the falling rate period were observed in size and water content variations with time. It was shown that the duration of the CRP decreases with increasing drying temperature.

The specific features of the neutron images of cylinders were discussed within the framework of MC results providing the parameterized description of the scattered distribution over the converter screen. The results of MC calculations are in good agreement with our experimental data.

References

1. Coulson JM, Richardson JF (1956) Chemical engineering. Vol. 2. Pergamon Press, London
2. Coussot P (2000) Scaling approach to the convective drying of a porous medium. Eur Phys J B 15:557–566
3. Czachor A, El-Ghany el Abd A, Milczarek JJ (2002) Determination of capillary motion of water in bricks using neutron radiography. Acta Phys Pol A 102:245–253
4. Czachor A, Milczarek JJ, Balasko M (2005) Neutron and gamma radiography station at the nuclear research reactor MARIA at Świerk. In: Chirco P, Rosa R (eds) Proc of the 7th World Conf on Neutron Radiography, 15–21 September, 2002, Rome, Italy. ENEA, Rome
5. Deinert MR, Parlange JY, Steenhuis T, Throop J, Ünlü K, Cady KB (2004) Measurement of fluid contents and wetting front profiles by real-time neutron radiography. J Hydrol 290:192–201
6. Domanus JC (ed) (1992) Practical neutron radiography. Kluwer Academic Publishers, Dordrecht
7. El-Ghany el Abd A, Czachor A, Milczarek JJ, Pogorzelski J (2005) Neutron radiography studies of water migration in construction porous materials. IEEE Trans Nucl Sci 52:299–304

8. El-Ghany el Abd A, Milczarek JJ (2004) Neutron radiography study of water absorption in porous building materials: anomalous diffusion analysis. J Phys D: Appl Phys 37:2305–2313

9. Hassanein R, de Beer F, Kardjilov N, Lehmann E (2006) Scattering correction algorithm for neutron radiography and tomography tested at facilities with different beam characteristics. Physica B 385/386:1194–1196

10. Hassanein R, Lehmann E, Vontobel P (2005) Methods of scattering corrections for quantitative neutron radiography. Nucl Instrum Methods A 542:353–360

11. Hassanein R, Meyer HO, Carminati A, Estermann M, Lehmann E, Vontobel P (2006) Investigations of water imbibition in porous stone by thermal neutron radiography. J Phys D: Appl Phys 39:4284–4291

12. Hibiki T, Mishima K (1996) Approximate method for measurement of phase-distribution in multiphase materials with small neutron-attenuation using a neutron beam as a probe. Nucl Instrum Methods A 324:345–351

13. Hutchings MT, Windsor CG (1987) Methods of experimental physics. Vol. 23, Part C. Academic Press, London

14. Kardjilov N, de Beer F, Hassanein R, Lehmann E, Vontobel P (2005) Scattering corrections in neutron radiography using point scattered function. Nucl Instrum Methods A 542:336–341

15. Keey RB (1972) Drying principles and practice. Pergamon Press, Oxford

16. Kowalski SJ (2003) Thermomechanics of drying processes. Springer, Berlin

17. Lehmann EH, Vontobel P, Kardjilov N (2004) Hydrogen distribution measurements by neutrons. Appl Radiat Isot 61:503–509

18. Milczarek JJ, Czachor A, El-Ghany el Abd A, Wiśniewski Z (2005) Dynamic neutron radiography observations of water migration in porous media. Nucl Instrum Methods A 542:232–236

19. Milczarek JJ, Fijał-Kirejczyk I, Żołądek J, Chojnowski M, Kowalczyk G (2008) Effect of gravitation on water migration in granular media. Acta Phys Pol A 113:1245–1254

20. Milczarek JJ, Trzciński A, El-Ghany el Abd A, Czachor A (2005) Monte Carlo code for neutron radiography. Nucl Instrum Methods A 542:237–240

21. Musielak G, Banaszak J (2007) Non-linear heat and mass transfer during convective drying of kaolin cylinder under non-steady conditions. Transp Porous Med 66:121–134

22. Tsimpanogiannis IN, Yortsos YC, Poulou S, Kanellopoulos N, Stubos AK (1999) Scaling theories of drying in porous medium. Phys Rev E 59:4353–4365

23. Unesaki H, Hibiki T, Mishima K (1998) Evaluation of scattered neutron component in thermal neutron radiography image: influence of scattered neutrons and unparallelness of incident neutron beam. Nucl Instrum Methods A 413:143–150

24. Yiotis AG, Tsimpanogiannis IN, Stubos AK, Yortsos YC (2006) Pore-network study of the characteristic periods in the drying of porous material. J Coll Interface Sci 297:738–748